BAP1 mutations define a specific subgroup of hepatocellular carcinoma with fibrolamellar features and PKA activation Short title: BAP1 HCC have FLC features and activate PKA

Theo Hirsch, Ana Negulescu, Barkha Gupta, Stefano Caruso, Bénédicte Noblet, Gabrielle Couchy, Quentin Bayard, Léa Meunier, Guillaume Morcrette, Jean-Yves Scoazec, et al.

BAP1 mutations define a specific subgroup of hepatocellular carcinoma with fibrolamellar features and PKA activation

Short title: **BAP1 HCC have FLC features and activate PKA**

Théo Z Hirsch*[1,2], Ana Negulescu*[1,2], Barkha Gupta[1,2], Stefano Caruso[1,2], Bénédicte Noblet[1,2], Gabrielle Couchy[1,2], Quentin Bayard[1,2], Léa Meunier[1,2], Guillaume Morcrette[1,2,3], Jean-Yves Scoazec[4], Jean-Frédéric Blanc[5,6,7], Giuliana Amaddeo[8], Jean-Charles Nault[1,2,9], Paulette Bioulac-Sage[6,7], Marianne Ziol[10], Aurélie Beaufrère[11], Valérie Paradis[11,12], Julien Calderaro[1,2,13], Sandrine Imbeaud[1,2], Jessica Zucman-Rossi**[1,2,14]

* Co-first authors, equally contributed
** Senior, corresponding author

1. Centre de Recherche des Cordeliers, Sorbonne Université, Inserm, Université de Paris, F-75006 Paris, France
2. Functional Genomics of Solid Tumors laboratory, équipe labellisée Ligue Nationale contre le Cancer, Labex OncoImmunology, F-75010, Paris, France
3. Service de Pathologie Pédiatrique, Assistance Publique Hôpitaux de Paris, Hôpital Robert Debré, F-75019 Paris, France.
4. Service d'anatomie et de cytologie pathologiques, Gustave Roussy Cancer Center, F-94800 Villejuif, France
5. Service Hépato-Gastroentérologie et Oncologie Digestive, Hôpital Haut-Lévêque, CHU de Bordeaux, F-33000 Bordeaux, France
6. Service de Pathologie, Hôpital Pellegrin, CHU de Bordeaux, F-33076 Bordeaux, France
7. Université Bordeaux, Inserm, Research in Translational Oncology, BaRITOn, F-33076 Bordeaux, France
8. Service d'Hépato-Gastro-Entérologie, Hôpital Henri Mondor, APHP, Université Paris Est Créteil, Inserm U955, Institut Mondor de Recherche Biomédicale, F-94010 Créteil, France
9. Service d'Hépatologie, Hôpital Jean Verdier, Hôpitaux Universitaires Paris-Seine-Saint-Denis, APHP, F-93140 Bondy, France
10. Service d'Anatomie Pathologique, Hôpital Jean Verdier, Hôpitaux Universitaires Paris-Seine-Saint-Denis, APHP, F-93140 Bondy, France
11. Service de pathologie, Hôpital Beaujon, APHP, F-92110 Clichy, France
12. Université Paris Diderot, CNRS, Centre de Recherche sur l'Inflammation (CRI), Paris, F-75890, France
13. Service d'Anatomopathologie, Hôpital Henri Mondor, APHP, Institut Mondor de Recherche Biomédicale, F-94010 Créteil, France
14. Hôpital Européen Georges Pompidou, APHP, F-75015 Paris, France

Contact information:
Jessica Zucman-Rossi; MD, PhD
Centre de recherche des Cordeliers
Functional genomics of solid tumors
15 rue de l'école de médecine
75006 Paris, France
TEL: +33 6 01 07 78 75
Email: jessica.zucman-rossi@inserm.fr

Disclosures:
Authors have no conflict of interest to declare.

Author contributions:
Study concept and design: JZR, TZH, AN. Acquisition of data: JZR, TZH, AN, BG, SC, BN, GC, QB, LM, GM, JYC, JFB, GA, JCN, PBS, MZ, AB, VP, JC, SI. Analysis and data interpretation: TZH, AN, SC, QB, LM, JZR. Manuscript writing: JZR, TZH, AN and all. Obtained funding: JZR.

Abbreviations:
BAP1: *BRCA1*-Associated Protein 1, cAMP: cyclic adenosine monophosphate, FLC: fibrolamellar carcinoma, HCC: hepatocellular carcinoma, MCP: Microenvironment Cell Populations, PKA: cAMP-dependent protein kinase, RNAseq: RNA-sequencing, (ss)GSEA: (single sample) gene set enrichment analysis, WES: whole exome sequencing, WGS: whole genome sequencing

Writing assistance: no writing assistance

1. Abstract

Background and aims: *DNAJB1-PRKACA* fusion is a specific driver event in fibrolamellar carcinoma (FLC), a rare subtype of hepatocellular carcinoma (HCC) occurring in adolescents and young adults. In older patients, molecular determinants of HCC with mixed histological features of HCC and FLC (mixed-FLC/HCC) remain to be discovered.

Methods: A series of 151 liver tumors including 126 HCC, 15 FLC, and 10 mixed-FLC/HCC were analyzed by RNAseq and whole-genome- or whole-exome-sequencing. Western-blots were performed to validate genomics discoveries. Results were validated using the TCGA database.

Results: Most of the mixed-FLC/HCC RNAseq clustered in a robust subgroup of 17 tumors all showing mutation or translocation inactivating *BAP1* that codes for the BRCA1 associated protein-1. Similar to FLC, BAP1-HCC were significantly enriched in female, tumor fibrosis and the lack of chronic liver disease when compared to non-BAP1-HCC. However, patients were older and with a poorer prognosis than FLC patients. BAP1 tumors were immune hot, showed progenitor features, did not show *DNAJB1-PRKACA* fusion and were almost all non-mutated for *CTNNB1*, *TP53* and *TERT* promoter. In contrast, 80% of the BAP1 tumors showed a chromosome gain of *PRKACA* at 19p13, combined with a loss of *PRKAR2A* (coding for the inhibitory regulatory subunit of PKA) at 3p21, leading to a high PRKACA/PRKAR2A ratio at the mRNA and protein levels.

Conclusion: We have characterized a subgroup of *BAP1*-driven HCC bearing fibrolamellar-like features and a dysregulation of the PKA pathway, which could be at the root of the clinical and histological similarities between BAP1 tumors and *DNAJB1-PRKACA* FLCs.

Key-words: liver cancer; fibrolamellar carcinoma; BAP1; PRKACA;

Lay summary:
- BAP1 inactivating alterations defined a homogeneous subgroup of hepatocellular carcinoma characterized by fibrolamellar-like features.
- These tumors are frequently developed in female, with non-cirrhotic liver
- Frenquent PKA activation and lymphocyte T infiltrates suggest that patients with BAP1 inactivated HCC could benefit from drug inactivating PKA and immuno-modulators.

Highlights
- BAP1 inactivated HCC are characterized by:
    - Fibrolamellar-like features including mixed-FLC/HCC
    - development in female with non-fibrotic liver
    - tumor fibrosis, T-cell infiltrates and tertiary lymphoid structures.
    - Frequent PKA activation
    - Hepato-pancreatic progenitor features
- Patients could benefit from PKA inhibitors and immuno-modulators

Graphical Abstract

Molecular HCC subgroups

	Fusion PRKACA	BAP1	non-BAP1/fusPRKACA
Major tumor subtype	Fibrolamellar	Mixed-Fibrolamellar	HCC
Liver background	F0-F1 No etiology	F0-F1 No etiology	F2-F4 Alcohol/HBV/HCV
Tumor histology	Fibrosis, perineural invasion		
		Steatosis, biliary tract inv., lympho T infiltr.	
Major gene alterations (PKA activation)	*DNAJB1-PRKACA* fusion (100%)	*BAP1* (100%) *PRKACA* gains (83%) *PRKAR2A* del (94%)	*TERT* (54%), *TP53* (40%), *CTNNB1* (35%) *GNAS* (1%)
Progenitor markers — Hepato-pancreatic	SOX 17, PDX1, HNF1β		
Cholangio-hepatic	EPCAM, VIM, THY1		Rare progenitor subtypes: EPCAM, THY1, GPC3, CK19
Pancreatic		IA1, PTF1α, NGN3	

Introduction

Fibrolamellar carcinoma (FLC) is a rare subtype of hepatocellular carcinoma (HCC) mostly diagnosed in adolescents and young adults. It was originally defined by specific histological features of both the tumor cells and their stroma, with the presence of abundant fibrosis arranged in a lamellar fashion around deeply eosinophilic large neoplastic hepatocytes, frequent central scar and calcifications[1,2]. FLC defines a specific subgroup of HCC since they have peculiar clinical features compared to classical HCC, such as a young age at onset between 10 to 35 years old, a balanced sex ratio, an absence of underlying liver disease or risk factors and a better prognosis with 80% of survival at 5-years after resection[3,4]. Biologically, FLCs show a high number of mitochondria and progenitor features, suggesting that the tumor cells are blocked at a specific stage of differentiation with hepatocellular (HEPAR1), biliary (CK7) and CD68 co-expressed markers[1,5]. In 2014, Honeyman and colleagues discovered a specific 400 kb chromosome deletion at chromosome 19 in FLC leading to recurrent chimeric *DNAJB1-PRKACA* gene fusion[6]. *DNAJB1* encodes HSP40, a member of the heat shock protein family, while *PRKACA* codes for the cAMP-dependent protein kinase (PKA) catalytic subunit alpha; the chimeric gene results in PRKACA catalytic domain overexpression and subsequent PKA activation. In addition, rare FLC without *DNAJB1-PRKACA* fusion were identified in patients with Carney disease due to *PRKAR1A* germline mutations leading also to PKA activation and similar phenotype[7]. In contrast, PKA activation is only rarely identified in HCC (<1% *GNAS* mutations) or in cholangiocarcinoma (around 6% of *GNAS* mutations and rare fusions of *PRKACA*, *PRKACAB* and *PRKAR1B*)[8,9].

Frequently, FLC diagnosis can be difficult and tumors with histological features of both HCC and FLC have been described as mixed-FLC/HCC[10-12]. In comparison with FLC, mixed-FLC/HCC patients were older, all above 35 years, and with a poor prognosis. Moreover, transcriptomic analyses showed a different profile of expression in the mixed-FLC and a lack of *DNAJB1-PRKACA* fusion[13,14]. Therefore, mixed-FLC/HCC should be better defined in the phenotypic/molecular diversity of the liver tumors, in particular to identify similarities and differences with FLC of the young and other HCC subtypes[12].

In this study, to identify specific molecular driver(s) of the mixed-FLC subgroup of tumors, we performed an integrated genomic analysis using RNA sequencing and whole-genome- or whole-exome-sequencing of 151 liver tumors classified in HCC, FLC and mixed-FLC/HCC by pathological reviewing.

Material and methods

Patients and tumors

We assembled a series of 151 patients (LICA-FR cohort) enriched with 15 FLC, 10 mixed FLC/HCC cases and including 126 HCC for controls[8,15], with genomic data (WGS or WES and RNAseq) and pathological reviewing (see below). The study was approved by the local Ethics Committee (CCPPRB Paris Saint-Louis IRB00003835), and informed consent was obtained in accordance with French legislation for all patients. Tumor and corresponding non-tumor samples were frozen at -80°C after tumor resection and all tumor samples were primary tumors except 8 samples collected at relapse; clinical features are summarized in Table 1. For validation, we used 345 tumors (339 HCC, 4 FLC, 2 mixed-FLC/HCC) from the TCGA (The Cancer Genome Atlas) cohort[16], whose clinical features are also described in Table 1.

Pathological reviewing

Multiple slides of the same tumor were reviewed by at least two liver pathologists for several histological criteria previously described[11,17,18] including: tumor differentiation (WHO grade and Edmonson grade), vascular invasion (microscopic), tumor architecture (macrotrabecular, microtrabecular, pseudoglandular), abundant fibrous stroma (>20%), steatosis, histological patterns (scirrhous, macrotrabecular massive), lymphocytic inflammation (>20%), tumor invasion (biliary tract, perineural) and clear cell presence. HCC containing at least one area with FLC features were annotated as mixed-FLC/HCC as previously described[11] (Supplementary Figure 1). For the TCGA cohort, histological features were reviewed by at least two liver pathologists from the virtual slides available online via cBioPortal (http://www.cbioportal.org/). Tertiary lymphoid structures were annotated on hematein-eosin-safran slides as in[19,20] for a subset of the LICA-FR cohort (55 tumors) and all tumors from the TCGA cohort.

Genomic sequencing

151 tumors and their corresponding non-tumor tissues were sequenced by whole exome sequencing (WES, n=115 including 43 new cases) or whole genome sequencing (WGS, n=36 including 3 new cases) as previously described[8,21,22]. For samples without WGS, targeted analysis of *TERT* promoter was performed with sanger (n=100) and/or miSeq (n=38) sequencing as previously described[8], while *BAP1* was re-sequenced with miSeq technology in 24 samples (the list of primer sequences is provided in Supplementary Table 1). Copy number analysis was performed as previously described[22] and manually corrected with the help of the GAP tool[23].

RNAseq and transcriptomic analyses

mRNAs were extracted from 151 tumor (including 64 new cases) and 3 non-tumor tissues and sequenced using Illumina TruSeq or Illumina TruSeq Stranded mRNA kit, libraries were sequenced by IntegraGen (Evry, France) on an Illumina HiSeq 2000 or 4000 paired-end 75 bp or 100 bp reads as previously described[24]. Fastq files were aligned to the reference human genome GRCh38 using TopHat2[25]. Reads mapping to multiple locations were removed and we used HTSeq[26] to obtain the number of reads associated to each gene in the Gencode v27 database, restricting to protein-coding genes, pseudogenes, antisense and lincRNAs (n=58288). We used the Bioconductor DESeq2 package[27] to import raw HTSeq counts for each sample into R statistical software and applied variance stabilizing transformation to the raw count matrix to obtain an expression matrix without variance-mean dependence (vst matrix). FPKM scores (number of fragments per kilobase

of exon model and millions of mapped reads) were calculated by normalizing the count matrix for the library size and the coding length of each gene. We used the area under the ROC curve (AUC) to identify and remove 2404 genes with a significant batch effect (AUC > 0.95 between one sequencing project and others). Unsupervised hierarchical clustering was done using Cosine distance and Ward method on most 5000 differentially expressed genes from the vst matrix as previously described[24].

Tumors were classified in the G1-G6 classification as previously described for the LICA-FR cohort[28] and the TCGA cohort[29]. We used the Bioconductor *limma* package[30] to test for differential gene expression between two groups of RNAseq samples of interest. All genes expressed in at least 5 samples (FPKM>0) were considered for the differential expression analysis. We applied a q-value threshold of ≤0.05 to define differentially expressed genes. We used an in-house adaptation of the GSEA method[31] to identify gene sets from the MSigDB (v. 6.0) database overrepresented among up- and down-regulated genes. Single sample GSEA scores were calculated as Gene Set Variation Analysis (GSVA) enrichment scores, using the GSVA package[32].

Relative abundance of immune and stromal cells infiltration within tumors was assessed through MCP scores computed with the Microenvironment Cell Populations-counter method[33] adapted to RNAseq data (exp matrix) after filtering out genes expressed in hepatocytes (the detailed list of genes used for each population is available in Supplementary Figure 2).

Immunoblotting

Protein were extracted from frozen tissues samples using modified Laemmli lysis buffer (50mM Tris pH=6.8, 2% SDS, 5% glycerol, 2mM DTT, 2.5mM EDTA/EGTA) supplemented with 2X phosphatase and protease inhibitor cocktail (#78444, Thermo Fisher Scientific, Waltham, MA, USA), 2mM Na_3VO_4 (#P0758S, BioLabs, Ipswich, MA, USA) and 10mM NaF (#674141, Sigma Aldrich, St. Louis, MO, USA), homogenized by Qiagen TissueLyser II and boiled for 10 minutes. Protein concentration was measured with the BCA assay kit (Pierce Biotechnology, Rockford, IL, USA). Equal amounts of protein were deposed on poly-acrylamide gel (Bio-Rad, Hercules, CA, USA), separated by electrophoresis, transferred on 0.2 μm nitrocellulose membrane (Bio-Rad) and incubated at 4°C with the following primary antibodies: anti-BAP1 (sc-28383 c4, Santa Cruz Biotechnologies, Dallas, TX, USA), anti-PKA-Cα (ab76238, Abcam, Cambridge, UK) and anti-PKA-R2 (ab32514, Abcam, Cambridge, UK) at 1:10000 dilution. Anti-mouse (#7076, Cell Signaling) or anti-rabbit (#7074, Cell Signaling) IgG horseradish peroxidase (HRP) linked secondary antibodies were used at 1:2000 dilution. Proteins were detected using SuperSignal West Pico Plus kit (#34580, Thermo Fisher Scientific) and signal was captured by ChemiDoc XRS system. Quantification was done by measuring the intensity of each band using Image Lab software (Bio-Rad) and normalised by the Ponceau whole lane charge evaluated with ImageJ software (National Institute of Health, Bethesda, MD, USA).

Immunohistochemistry

Immunohistochemistry was performed on formalin-fixed paraffin-embedded tumor tissues with the Leica Bond automated stainer. The percentage of EpCAM positive tumor cells was assessed in 52 tumors from the LICA-FR series stained with an EpCAM monoclonal antibody (Ber-Ep4). Quantitative scores of infiltration by T cells and B cells were assessed in 41 tumors with antibodies against CD3 (Dako, Santa Clara, California, Clone F7.2.38, dilution 1/50) and CD20 (Dako, Clone L26, Dilution 1/500) respectively,

with a separate estimation of positive cells within the tumor stroma and within the tumor parenchyma.

Statistical analysis

For statistical analysis of gene expression data, R version 3.3.2 (R Development Core Team, R: A language and environment for statistical computing. R Foundation for Statistical Computing, Vienna, http://www.R-project.org) and Bioconductor version 3.4 were used. Wilcoxon, Fisher or χ^2 statistical tests were applied with respect to the type of variable. Survival analysis was performed in patients treated by R0 liver resection (n=112) as previously described[8] including 5 FLC patients without good quality RNAseq data available. We assessed overall survival defined by the interval between surgery and death whatever the cause and survival curves were represented using the Kaplan-Meier method compared with the Log Rank test. Univariate analysis was performed using the Cox model. A p value < 0.05 was considered as significant.

Data availability

The sequencing data of the LICA-FR cohort reported in this paper have been deposited to the EGA (European Genome-phenome Archive) database (RNA-seq accession [EGAS00001002879], [EGAS00001001284] and [EGAS00001003837]; WES accessions [EGAS00001000217], [EGAS00001001002], [EGAS00001003063], [EGAS00001000679] and [EGAS00001003837]; WGS accessions [EGAS00001002408], [EGAS00001000706], [EGAS00001002888] and [EGAS00001003837]), through the ICGC (International Cancer Genome Consortium) data access committee. The sequencing data from the TCGA cohort were retrieved from http://www.cbioportal.org/.

Results

FLC and mixed-FLC/HCC cluster into two distinct transcriptomic subgroups of tumors.

We performed RNA sequencing of 151 liver tumor samples which included 126 HCC, 15 FLC and 10 mixed-FLC/HCC, defined by pathological reviewing (Supplementary Figure 1) and with clinical features described in Table 1. All FLC but two clustered in a robust subgroup of 15 tumors together with two mixed-FLC/HCC (Figure 1). Interestingly, all 15 patients of this cluster were young (age min=17 years; max=36 years, mean=26 years) and all the tumors harbored the *DNAJB1-PRKACA* fusion (Figure 1). Six out of the 8 remaining mixed-FLC/HCC clustered in a second group of tumors also including 2 FLC and 9 HCC (Figure 1). This cluster of 17 tumors highly enriched in mixed-FLC/HCC was located in proximity to the FLC cluster, but patients were older (age min=27 years; max=73 years, mean=51 years) including the 2 FLC that developed at 51 years and 65 years. Interestingly all the 17 tumors lacked the *DNAJB1-PRKACA* fusion but showed alterations in the *BAP1* gene. Only one HCC mutated for *BAP1* (#794T), without FLC features, was outside this FLC/HCC cluster. Finally, only 2 mixed-FLC/HCC, not mutated for BAP1 nor harboring *DNAJB1-PRKACA* fusion, were distributed outside the two clusters (Figure 1).

In agreement with the tumor suppressor function of BAP1 in various tumor types[16,34–37], *BAP1* alterations were predicted to inactivate the gene either by somatic mutations (9 frameshift, 2 nonsense, 1 splice site, 2 missense and 1 nonstop), by gene fusion in two cases (*DAG1-BAP1* in #3919T and a complex event leading to both *BAP1-LINCO1460* and *RAB3GAP1-BAP1* fusions in #4211T, see Supplementary Figure 3), or by homozygous deletion in 2 tumors (Table 2). In all tumors, *BAP1* alterations were biallelic with two mutations in one case (#2211T) or a deletion of the second allele of *BAP1* (Table 2).

Since no FLC carrying the *DNAJB1-PRKACA* fusion showed *BAP1* alteration, we define 3 distinct groups of tumors: altered for *BAP1* (BAP1 tumors), with *DNAJB1-PRKACA* fusion (fusPRKACA tumors) or without either alterations (non-BAP1/fusPRKACA tumors), as represented in Figure 1 (Molecular group annotation).

BAP1 altered hepatocellular carcinomas show distinct clinical and histological features

In our cohort LICA-FR, patients with BAP1 tumors (n=18) were younger (median 51 years) than non-BAP1/fusPRKACA patients (n=118, median 64 years, p=0.006) but older than fusPRKACA patients (n=15, median 26 years, p=3.3e-6, Figure 2A). Compared to non-BAP1/fusPRKACA patients, BAP1 patients were enriched in females (67% vs 19%, p=9.7e-5), in non-fibrotic liver (F0-F1), without known etiologies of HCC (50% vs 12%, p=0.0008, Figure 2C-E and Table 1). Patients with BAP1 tumors showed similar overall survival compared to non-BAP1/fusPRKACA HCC whereas fusPRKACA patients showed a better prognosis (p=0.02 in log-rank test, Figure 2B). All of these clinical relations, except younger age, were also found in the TCGA cohort that included 16 BAP1 tumors and 6 fusPRKACA tumors out of 345 HCC (Figure 2A-E and Table 1). Of note, a 67-years old female patient in TCGA harbored both *DNAJB1-PRKACA* fusion and *BAP1* mutation in the tumor, this case was excluded from the statistical analysis.

BAP1 tumors were enriched in mixed-FLC/HCC (6 out of 18), characterized by an abundant fibrous stroma (72%), intratumor steatosis (67%), biliary tract invasion (31%), perineural invasion (13%), and a high lymphocytic infiltration (73%) (Figure 1 & 2F-J, Table 1). Tertiary lymphoid structures were frequently identified in BAP1 tumors (70%) ranging from simple aggregate up to secondary follicles harboring a clear germinal center as previously described in HCC[20] (Figure 2K). The Microenvironment Cell Populations-

counter method[33] applied to RNAseq data showed a high component of the microenvironment in *BAP1* tumors, enriched in T and B lymphocytes, endothelial cells and myeloid dendritic cells when compared with non-BAP1/fusPRKACA tumors (Figure 2L, Supplementary Figure 2). In accordance with these results, CD3 immunohistochemistry revealed a higher infiltration of T cells in the stroma of BAP1 tumors compared to non-BAP1/fusPRKACA (Figure 2M, N). Infiltrated CD20+ B cells were also observed within BAP1 tumors but in levels comparable to non-BAP1/fusPRKACA HCC (Figure 2O and Supplementary Figure 2). In the TCGA cohort, we confirmed that BAP1 tumors were highly fibrous, steatotic, enriched in perineural invasion and with frequent lymphocytic infiltration organized in tertiary lymphoid structures (Figure 2F-K and Table 1).

BAP1 tumors demonstrate a specific genomic profile with frequent *PRKACA* gain and *PRKAR2A* deletion

Analysis of the profile of gene mutations and chromosome alterations in BAP1 tumors showed a significant exclusion from alterations in the 3 most frequent drivers of HCC, namely *TERT* promoter, *CTNNB1* and *TP53*[22] (Figure 1 and Table 1). This exclusion was confirmed in the TCGA cohort and also observed in *DNAJB1-PRKACA* fusion tumors (Figure 1 and Table 1). In contrast, BAP1 tumors were slightly enriched in *RB1*, *KMT2D*, *ATM* and *ALB* mutations (n=3 for each gene, Figure 1) but these associations did not reach significance.

In order to find alternative driver events associated to *BAP1* alterations in HCC, we compared the frequency of copy-number alterations between the 3 molecular groups of tumors. In 15 out of the 18 BAP1 tumors (83%) we identified a specific recurrent chromosome gain at the 19p13 locus centered on the *PRKACA* gene found in only 6% of the non-BAP1/fusPRKACA tumors (p=3e-12) and in none of the fusPRKACA tumors (Figure 3A-B). In addition, deletions at chromosome 3p21 identified in the BAP1 tumors encompassed both *BAP1* and *PRKAR2A* (coding for PKA-R2α, a negative regulatory subunit of the cAMP-dependent protein kinase PKA) genes distant by 3.5 Mb (94% vs 4% in non-BAP1/fusPRKACA tumors, p=2e-16, Figure 3A-B and Supplementary Figure 4). In agreement with these findings, RNAseq data showed a significant lower *PRKAR2A* and higher *PRKACA* gene expression in BAP1 tumors compared to non-BAP1/fusPRKACA tumors and these results were confirmed at the protein level (Figure 3B,D-F). A significant increased ratio of PRKACA to PKA-R2 proteins, reflecting PKA activity, was monitored in both BAP1 and fusPRKACA groups of tumors compared to non-BAP1/fusPRKACA HCC (Figure 3H). Accordingly, PKA activity assessed by single sample Gene Set Enrichment Analysis (ssGSEA) was increased in both BAP1 and fusPRKACA tumors (Figure 3C).

These results suggest that similarly to FLC with *DNAJB1-PRKACA* fusion, the PKA pathway is activated in BAP1 tumors but with an alternative mechanism associating *PRKACA* chromosome gains and *PRKAR2A* deletions (Supplementary Figure 4).

BAP1 and *DNAJB1-PRKACA* tumors share common proliferation and differentiation programs, distinct from other hepatocellular tumors

At the transcriptomic level, 78% of the BAP1 tumors were classified in the G1 sub-group of HCC, known to be associated with progenitor features[17,28], compared to only 11% of the non-BAP1/fusPRKACA tumors (p=9.5e-9) and 20% of the fusPRKACA FLC and these results were confirmed in TCGA (63% vs 14%, p=7.0e-5, Table 1). Single sample GSEA (ssGSEA) revealed that BAP1 and fusPRKACA tumors were highly enriched in stem cell

and neuronal features, vasculature development, extracellular matrix and epithelial-mesenchymal transition compared to the non-BAP1/fusPRKACA HCCs (Figure 4A). FusPRKACA tumors appeared to be less proliferative than non-BAP1/fusPRKACA tumors, as illustrated by lower levels of cell cycle genes such as *CCNB1*, *PCNA* or *BIRC5*, while the tendency toward a low proliferation in BAP1 tumors did not reach significance (Figure 4B).

Interestingly, expression of the 3 TGF-β ligands was increased in both BAP1 and fusPRKACA tumors (Figure 4B) together with an enrichment in the signature of TGF-β signaling in fibroblasts (Plasari TGFb1 Targets 10hr Up, Figure 4A). In contrast, signature of TGF-β activation in hepatocytes defined by Coulouarn et al[38] was not retrieved neither in BAP1 nor in fusPRKACA tumors, suggesting that an activation of the TGF-β pathway in fibroblasts but not in tumor hepatocellular cells could be at the root of the fibrotic phenotype in both groups of tumors.

In accordance with the enrichment in stem cell features detected by GSEA, BAP1 and fusPRKACA tumors shared high expression of hepatic stem cell genes such as *EPCAM*, *VIM* or *THY1* (CD90) (Figure 4B). Immunohistochemistry performed on a subset of tumors confirmed the higher percentage of EpCAM positive progenitor cells within both BAP1 tumors and fusPRKACA tumors while this staining was absent in a vast majority of non-BAP1/fusPRKACA tumors (Figure 4C, D). Furthermore, we also monitored high expressions of markers of the common hepato-pancreatic progenitor[39,40] such as *PDX1* or *SOX17* (Figure 4B), 2 markers which have previously been detected by immunohistochemistry in a majority of FLC samples[5] . Among the differentiation markers, we observed a significant decrease of hepatocyte specific genes *ALB, PROX* or *HNF4A* and a significant increase of cholangiocyte specific gene *KRT7* in fusPRKACA compared to BAP1 or non-BAP1/fusPRKACA tumors (Supplementary Figure 5). Also, several markers of pancreatic lineage were overexpressed in BAP1 and/or fusPRKACA tumors, but at various levels in the 2 groups of tumors. For instance, among the pancreatic markers, a high expression of *PDX1*, *PAX6*, *PAK3*, and *MNX1* was identified in BAP1 and fusPRKACA tumors while *NEUROG3* (NGN3), *INSM1* (IA-1), *PTF1A, TRIM50, GP2* and *TGIF2* overexpression was restricted to BAP1 tumors and only fusPRKACA tumors overexpressed the pancreatic/neuroendocrine gene *PCSK1* (Figure 4B and Supplementary Figure 5). Other neuroendocrine genes such as *CALCA, NTS, DNER* or *SSTR5* were overexpressed with different patterns in the two groups of tumors (Supplementary Figure 5). Moreover, we observed a high expression of genes coding for proteins involved in neural infiltration and guidance, such as neuron guide molecules (*NGF*, *NTF3*, *BDNF*) and their binding receptors expressed on neurons (TrkA-C (*NTRK1-3*) and p75NTR (*NFGR*), Supplementary Figure 5), possibly accounting for the enrichment in perineural invasion in both BAP1 and fusPRKACA tumors (Figure 2I). In line with a possible neural infiltration, other neuron expressed receptors such as UNC5A-D were found significantly overexpressed in BAP1 or fusPRKACA tumors (Supplementary Figure 5).

Lastly, the higher expression of the hepato-pancreatic progenitor marker PDX1 and the lack of expression of pancreatic committed progenitor markers such as IA-1 or PTF1A in fusPRKACA compared to BAP1 tumors, suggest a hepato-pancreatic progenitor-like program in fusPRKACA tumors and a more pancreatic engaged program in BAP1 tumors (Figure 4B and Figure 5).

Discussion

In this study, we showed that *BAP1* alterations delineate a specific subgroup of HCC with common clinical, histological and molecular features (Figure 5A). BAP1 is a deubiquitinating enzyme active in both the cytosol, where it controls the stability of different proteins, and in the nucleus, where it targets H2A histones as part of the Polycomb group repressive deubiquitinase complex, which is involved in development and stem cell pluripotency[41,42]. BAP1 is described as a tumor suppressor since it is lost in different tumors including cholangiocarcinoma (around 25%) and HCC (around 5%)[16,34–37]. However BAP1 was recently shown to also have an anti-apoptotic role in the liver[42], which could explain our observation of an increased expression of *BAP1* in HCC compared to normal liver (Figure 3B,D-E). Here, we found that the BAP1 tumors include most of the mixed FLC-HCC tumors and show several clinical and histological similarities with the classical FLC together with a common PKA pathway activation.

Fibrolamellar features in liver tumors are already known to be related to PKA activation through 3 different mechanisms: (i) the *DNAJB1-PRKACA* fusion in FLC [6], (ii) inactivating mutations in *PRKAR1A* in rare FLC developed in Carney complex patients[7] and (iii) activating mutations in *GNAS* (leading to production of cAMP and subsequent activation of PKA) identified in rare hepatocellular adenomas characterized by fibrolamellar-like patterns[43]. Here, we discovered a fourth mechanism of PKA activation in BAP1 tumors resulting from recurrent gains of *PRKACA* and deletions of *PRKAR2A*, encoding respectively a catalytic subunit and an inhibitory regulatory subunit of PKA, with consequences at the mRNA and protein levels (Figure 3 and Supplementary Figure 4).

An important characteristic of the *DNAJB1-PRKACA* and BAP1 tumors is their age distribution starting with FLC in the second and third decade, then BAP1 HCC occurring before non-BAP1/fusPRKACA HCC (Figure 5A). This gradient could be related to the cell of origin of the malignant transformation since FLC has been proposed to originate from the biliary tree stem cell[5], a recently discovered hepato-pancreatic progenitor[39,40], in agreement with the hepato-pancreatic progenitor phenotype we identified in both fusPRKACA and BAP1 tumors (Figure 5B). BAP1 loss may promote a dedifferentiation towards a progenitor phenotype since *BAP1* silencing in Huh7 HCC cell line induces an increase in stemness markers expression such as *EPCAM* or *PROM1*[44]. Similarly, CRISPR-based loss of *BAP1* in human liver organoids increases the expression of progenitor markers while reducing markers of liver function and ultimately epithelial homeostasis, possibly via a direct regulation of transcription by BAP1 through its known role in the Polycomb deubiquitinase complex[42]. In the TCGA cohort, the unique patient with HCC harboring both *DNAJB1-PRKACA* fusion and *BAP1* inactivation was old (67y) suggesting that the progenitor phenotype induced by BAP1 loss could be required for the oncogenic effect of PKA activation in an old liver. This is in line with our observation of a co-occurrence of BAP1 inactivation and PKA activation through copy number alterations. Remarkably, 2 independent teams recently reported the presence of *DNAJB1-PRKACA* fusions in rare pancreatic and biliary neoplasms, thus reinforcing the link between the oncogenic activation of PKA and the hepato-pancreatic progenitor lineage, while challenging the exclusivity between FLC and the *DNAJB1-PRKACA* fusion[45,46].

Of note, HCC usually lacks lymph node involvement or perineural invasion, commonly found in other epithelial tumors such as pancreatic adenocarcinomas[47,48] or cholangiocarcinoma[49,50]. Conversely, there is a high rate of lymph node metastasis in FLC (up to 70%)[51] and here we identified an enrichment of perineural invasion in BAP1 and

fusPRKACA tumors across the 2 series (Table 1). This enrichment could be a consequence of the overexpression of genes encoding neuron guide molecules (*NGF*, *NTF3*, *BDNF*) that allow the recruitment and growth of neurons expressing axonal guidance receptors (TrkA-C, p75NTR, UNC5A-D, see Supplementary Figure 5).

Strikingly, BAP1 tumors are never mutated in the *TERT* promoter (in both LICA-FR and TCGA cohort) while this alteration is found in 30-60% of HCC[16,52]. This could also be a consequence of the progenitor state of the tumor cells associated with BAP1 loss, since *in vitro* experiments suggest that *BAP1* overexpression can repress *TERT* transcription[53] and progenitors cells are supposed to maintain their telomeres throughout replication without requiring mutations. This would also explain the exclusion between *DNAJB1-PRKACA* fusion and *TERT* alteration, following the hypothesis that the cell of origin of FLC is a progenitor[5].

While it has been suggested that endocrine/pancreatic features were specific of FLC and not found in mixed-FLC/HCC[13], here we show that both fusPRKACA and BAP1 tumors express high levels of neuroendocrine and pancreatic markers but with different patterns (Supplementary Figure 5). These different profiles of expression could reflect different stages of differentiation along the hepato-pancreatic lineage in the 2 groups of tumors as a consequence of their different cell of origin, as discussed above (Figure 5B). Moreover, an association between neuroendocrine features and abundant fibrous stroma has already been described[54].

Interestingly, *BAP1* mutations are recurrently identified in several tumor types including uveal or cutaneous melanoma, mesothelioma, renal cell carcinoma, mesothelioma and lung cancers[55]. In 2013, a pan-cancer study has defined a typical morphology of *BAP1*-mutated cells as "rounded or polygonal cell shape with abundant amphophilic or eosinophilic cytoplasm"[56]. Interestingly, these features are also retrieved in FLC[1,4] as well as in BAP1 liver tumors (in both FLC and HCC components). This, along with the abundant fibrous stroma, hinders the distinction between BAP1 and fusPRKACA tumors based solely on histology in our cohort of tumors and in other reports[13,57]. These observations argue for the use of molecular characterization to distinguish BAP1 tumors not only from the fusPRKACA FLC but also from scirrhous HCC, another type of highly fibrous liver tumors usually not mutated in BAP1 (Figure 1 and Table 1). However, it is worth noting that the detection of *BAP1* mutations is challenging due to the high level of stromal contamination: in our series, 3 out of the 15 *BAP1* mutations were not found at first in the analysis of whole exome data, but were later detected in target sequencing of *BAP1* with a higher depth.

In a clinical perspective, our observations of similarities between fusPRKACA and BAP1 tumors may be in favor of developing common therapeutic strategies. Indeed, the over-activation of PKA in both groups of tumors argues that potential future treatments targeting PKA, if successful in FLC, could be repositioned to also combat BAP1 tumors. In a therapeutic perspective, the 2 groups of tumors could benefit from anti-angiogenic drugs such as sorafenib[58] due to their common enrichment in markers of angiogenesis and endothelial cells (Figure 4A and Supplementary Figure 2). Of note, a link between *BAP1* alterations and angiogenesis was also recently described in uveal melanoma[59]. Finally, as BAP1 HCC are highly infiltrated by lymphocytes (Figure 2J), a feature also described in *BAP1* mutated peritoneal mesothelioma[60], they can be considered as good candidates for immunotherapy. Of note, despite this higher lymphocytic infiltration, we did not monitor a difference in the tumor mutational burden of BAP1 tumors compared

to non-BAP1/fusPRKACA tumors, while both groups of tumors had more mutations than fusPRKACA tumors (Supplementary Figure 2B).

In conclusion, we characterized a new molecular subgroup of HCC, driven by *BAP1* loss of function and PKA activation in a context of a hepato-pancreatic progenitor de-differentiation, associated to specific pathological subtype of tumors including abundant fibrous stroma, steatosis, lymphocyte infiltration, perineural and biliary track invasion developed mainly in female patients without cirrhosis and chronic liver disease.

2. References

1. Craig JR, Peters RL, Edmondson HA, et al. Fibrolamellar carcinoma of the liver: a tumor of adolescents and young adults with distinctive clinico-pathologic features. Cancer 1980;46:372–9.

2. Edmondson HA. Differential diagnosis of tumors and tumor-like lesions of liver in infancy and childhood. AMA J Dis Child 1956;91:168–86.

3. Kassahun WT. Contemporary management of fibrolamellar hepatocellular carcinoma: diagnosis, treatment, outcome, prognostic factors, and recent developments. World J Surg Oncol 2016;14:151.

4. Lin C-C, Yang H-M. Fibrolamellar Carcinoma: A Concise Review. Arch Pathol Lab Med 2018;142:1141–1145.

5. Oikawa T, Wauthier E, Dinh TA, et al. Model of fibrolamellar hepatocellular carcinomas reveals striking enrichment in cancer stem cells. Nat Commun 2015;6:8070.

6. Honeyman JN, Simon EP, Robine N, et al. Detection of a recurrent DNAJB1-PRKACA chimeric transcript in fibrolamellar hepatocellular carcinoma. Science 2014;343:1010–4.

7. Graham RP, Lackner C, Terracciano L, et al. Fibrolamellar carcinoma in the Carney complex: PRKAR1A loss instead of the classic DNAJB1-PRKACA fusion. Hepatology 2018;68:1441–1447.

8. Nault J-C, Martin Y, Caruso S, et al. Clinical impact of genomic diversity from early to advanced hepatocellular carcinoma. Hepatology 2019.

9. Nakamura H, Arai Y, Totoki Y, et al. Genomic spectra of biliary tract cancer. Nat Genet 2015;47:1003–10.

10. Malouf G, Falissard B, Azoulay D, et al. Is histological diagnosis of primary liver carcinomas with fibrous stroma reproducible among experts? J Clin Pathol 2009;62:519–24.

11. Malouf GG, Brugières L, Deley M-C Le, et al. Pure and mixed fibrolamellar hepatocellular carcinomas differ in natural history and prognosis after complete surgical resection. Cancer 2012;118:4981–90.

12. Calderaro J, Ziol M, Paradis V, et al. Molecular and histological correlations in liver cancer. J Hepatol 2019;71:616–630.

13. Malouf GG, Job S, Paradis V, et al. Transcriptional profiling of pure fibrolamellar hepatocellular carcinoma reveals an endocrine signature. Hepatology 2014;59:2228–37.

14. Malouf GG, Tahara T, Paradis V, et al. Methylome sequencing for fibrolamellar hepatocellular carcinoma depicts distinctive features. Epigenetics 2015;10:872–81.

15. Nault JC, Reyniès A De, Villanueva A, et al. A hepatocellular carcinoma 5-gene score associated with survival of patients after liver resection. Gastroenterology 2013;145:176–187.

16. Ally A, Balasundaram M, Carlsen R, et al. Comprehensive and Integrative Genomic Characterization of Hepatocellular Carcinoma. Cell 2017;169:1327-1341.e23.

17. Calderaro J, Couchy G, Imbeaud S, et al. Histological subtypes of hepatocellular carcinoma are related to gene mutations and molecular tumour classification. J Hepatol 2017;67:727–738.

18. Ziol M, Poté N, Amaddeo G, et al. Macrotrabecular-massive hepatocellular carcinoma: A distinctive histological subtype with clinical relevance. Hepatology 2018;68:103–112.

19. Murakami J, Shimizu Y, Kashii Y, et al. Functional B-cell response in intrahepatic lymphoid follicles in chronic hepatitis C. Hepatology 1999;30:143–50.

20. Calderaro J, Petitprez F, Becht E, et al. Intra-tumoral tertiary lymphoid structures are associated with a low risk of early recurrence of hepatocellular carcinoma. J Hepatol 2019;70:58–65.

21. Guichard C, Amaddeo G, Imbeaud S, et al. Integrated analysis of somatic mutations and focal copy-number changes identifies key genes and pathways in hepatocellular carcinoma. Nat Genet 2012;44:694–698.

22. Schulze K, Imbeaud S, Letouzé E, et al. Exome sequencing of hepatocellular carcinomas identifies new mutational signatures and potential therapeutic targets. Nat Genet 2015;47:505–511.

23. Popova T, Manié E, Stoppa-Lyonnet D, et al. Genome Alteration Print (GAP): a tool to visualize and mine complex cancer genomic profiles obtained by SNP arrays. Genome Biol 2009;10:R128.

24. Bayard Q, Meunier L, Peneau C, et al. Cyclin A2/E1 activation defines a hepatocellular carcinoma subclass with a rearrangement signature of replication stress. Nat Commun 2018;9:5235.

25. Kim D, Pertea G, Trapnell C, et al. TopHat2: accurate alignment of transcriptomes in the presence of insertions, deletions and gene fusions. Genome Biol 2013;14:R36.

26. Anders S, Pyl PT, Huber W. HTSeq--a Python framework to work with high-throughput sequencing data. Bioinformatics 2015;31:166–9.

27. Love MI, Huber W, Anders S. Moderated estimation of fold change and dispersion for RNA-seq data with DESeq2. Genome Biol 2014;15:550.

28. Boyault S, Rickman DS, Reyniès A De, et al. Transcriptome classification of HCC is related to gene alterations and to new therapeutic targets. Hepatology 2007;45:42–52.

29. Calderaro J, Meunier L, Nguyen CT, et al. ESM1 as a marker of macrotrabecular-massive hepatocellular carcinoma. Clin Cancer Res 2019.

30. Ritchie ME, Phipson B, Wu D, et al. limma powers differential expression analyses for RNA-sequencing and microarray studies. Nucleic Acids Res 2015;43:e47.

31. Subramanian A, Tamayo P, Mootha VK, et al. Gene set enrichment analysis: a knowledge-based approach for interpreting genome-wide expression profiles.

Proc Natl Acad Sci U S A 2005;102:15545–50.

32. Hänzelmann S, Castelo R, Guinney J. GSVA: gene set variation analysis for microarray and RNA-seq data. BMC Bioinformatics 2013;14:7.

33. Becht E, Giraldo NA, Lacroix L, et al. Estimating the population abundance of tissue-infiltrating immune and stromal cell populations using gene expression. Genome Biol 2016;17:218.

34. Harbour JW, Onken MD, Roberson EDO, et al. Frequent mutation of BAP1 in metastasizing uveal melanomas. Science 2010;330:1410–3.

35. Bott M, Brevet M, Taylor BS, et al. The nuclear deubiquitinase BAP1 is commonly inactivated by somatic mutations and 3p21.1 losses in malignant pleural mesothelioma. Nat Genet 2011;43:668–72.

36. Peña-Llopis S, Vega-Rubín-de-Celis S, Liao A, et al. BAP1 loss defines a new class of renal cell carcinoma. Nat Genet 2012;44:751–9.

37. Jiao Y, Pawlik TM, Anders RA, et al. Exome sequencing identifies frequent inactivating mutations in BAP1, ARID1A and PBRM1 in intrahepatic cholangiocarcinomas. Nat Genet 2013;45:1470–1473.

38. Coulouarn C, Factor VM, Thorgeirsson SS. Transforming growth factor-β gene expression signature in mouse hepatocytes predicts clinical outcome in human cancer. Hepatology 2008;47:2059–2067.

39. Cardinale V, Wang Y, Carpino G, et al. Multipotent stem/progenitor cells in human biliary tree give rise to hepatocytes, cholangiocytes, and pancreatic islets. Hepatology 2011;54:2159–72.

40. Lanzoni G, Cardinale V, Carpino G. The hepatic, biliary, and pancreatic network of stem/progenitor cell niches in humans: A new reference frame for disease and regeneration. Hepatology 2016;64:277–86.

41. Scheuermann JC, Ayala Alonso AG de, Oktaba K, et al. Histone H2A deubiquitinase activity of the Polycomb repressive complex PR-DUB. Nature 2010;465:243–7.

42. Artegiani B, Voorthuijsen L van, Lindeboom RGH, et al. Probing the Tumor Suppressor Function of BAP1 in CRISPR-Engineered Human Liver Organoids. Cell Stem Cell 2019:1–17.

43. Nault JC, Fabre M, Couchy G, et al. GNAS-activating mutations define a rare subgroup of inflammatory liver tumors characterized by STAT3 activation. J Hepatol 2012;56:184–91.

44. Woo HG, Choi J-H, Yoon S, et al. Integrative analysis of genomic and epigenomic regulation of the transcriptome in liver cancer. Nat Commun 2017;8:839.

45. Vyas M, Hechtman JF, Zhang Y, et al. DNAJB1-PRKACA fusions occur in oncocytic pancreatic and biliary neoplasms and are not specific for fibrolamellar hepatocellular carcinoma. Mod Pathol 2019.

46. Singhi AD, Wood LD, Parks E, et al. Recurrent Rearrangements in PRKACA and PRKACB in Intraductal Oncocytic Papillary Neoplasms of the Pancreas and Bile Duct. Gastroenterology 2019.

47. Liu B, Lu K-Y. Neural invasion in pancreatic carcinoma. Hepatobiliary Pancreat Dis Int 2002;1:469–76.

48. Winter JM, Cameron JL, Campbell KA, et al. 1423 pancreaticoduodenectomies for pancreatic cancer: A single-institution experience. J Gastrointest Surg 2006;10:1199–210; discussion 1210-1.

49. Bhuiya MR, Nimura Y, Kamiya J, et al. Clinicopathologic studies on perineural invasion of bile duct carcinoma. Ann Surg 1992;215:344–9.

50. Pichlmayr R, Weimann A, Klempnauer J, et al. Surgical treatment in proximal bile duct cancer. A single-center experience. Ann Surg 1996;224:628–38.

51. Yamashita S, Vauthey J-N, Kaseb AO, et al. Prognosis of Fibrolamellar Carcinoma Compared to Non-cirrhotic Conventional Hepatocellular Carcinoma. J Gastrointest Surg 2016;20:1725–31.

52. Nault J-C, Ningarhari M, Rebouissou S, et al. The role of telomeres and telomerase in cirrhosis and liver cancer. Nat Rev Gastroenterol Hepatol 2019;8:294–296.

53. Linne H, Yasaei H, Marriott A, et al. Functional role of SETD2, BAP1, PARP-3 and PBRM1 candidate genes on the regulation of hTERT gene expression. Oncotarget 2017;8:61890–61900.

54. Laskaratos F-M, Rombouts K, Caplin M, et al. Neuroendocrine tumors and fibrosis: An unsolved mystery? Cancer 2017;123:4770–4790.

55. Masoomian B, Shields JA, Shields CL. Overview of BAP1 cancer predisposition syndrome and the relationship to uveal melanoma. J Curr Ophthalmol 2018;30:102–109.

56. Murali R, Wiesner T, Scolyer RA. Tumours associated with BAP1 mutations. Pathology 2013;45:116–26.

57. Griffith OL, M.Griffith, K.Krysiak, et al. A genomic case study of mixed fibrolamellar hepatocellular carcinoma. Ann Oncol 2016;27:1148–1154.

58. Wilhelm SM, Adnane L, Newell P, et al. Preclinical overview of sorafenib, a multikinase inhibitor that targets both Raf and VEGF and PDGF receptor tyrosine kinase signaling. Mol Cancer Ther 2008;7:3129–40.

59. Brouwer NJ, Gezgin G, Wierenga APA, et al. Tumour Angiogenesis in Uveal Melanoma Is Related to Genetic Evolution. Cancers (Basel) 2019;11:1–12.

60. Shrestha R, Nabavi N, Lin Y-Y, et al. BAP1 haploinsufficiency predicts a distinct immunogenic class of malignant peritoneal mesothelioma. Genome Med 2019;11:8.

Table 1: Clinical, histological and molecular features of tumors stratified by molecular alterations

		LICA-FR non-BAP1/fusPRKACA tumors (n=118)	BAP1 tumors (n=18)		fusPRKACA tumors (n=15)		TCGA non-BAP1/fusPRKACA tumors (n=323)	BAP1 tumors (n=16)		fusPRKACA tumors (n=6)	
		n/ntot (%)	n/ntot (%)	p-val	n/ntot (%)	p-val	n/ntot (%)	n/ntot (%)	p-val	n/ntot (%)	p-val
Histological Diagnosis	HCC	116/118 (98)	10/18 (56)	***###	0/15 (0)	⊹⊹⊹	323/323 (100)	16/16 (100)	###	0/6 (0)	⊹⊹⊹
	FLC	0/118 (0)	2/18 (11)	*###	13/15 (87)	⊹⊹⊹	0/323 (0)	0/16 (0)	##	4/6 (67)	⊹⊹⊹
	mixed FLC/HCC	2/118 (2)	6/18 (33)	***	2/15 (13)		0/323 (0)	0/16 (0)		2/6 (33)	⊹⊹⊹
Age at sampling (years)		64 (18-90)	51 (27-73)	**###	26 (17-36)	⊹⊹⊹	61 (20-90)	61 (44-77)	###	22 (17-35)	⊹⊹⊹
Female gender		23/118 (19)	12/18 (67)	***	9/15 (60)	⊹⊹	92/323 (28)	12/16 (75)	***	3/6 (50)	
Alcohol intake		47/116 (41)	5/16 (31)		0/12 (0)	⊹⊹	107/304 (35)	3/14 (21)		1/4 (25)	
Hepatitis B		39/118 (33)	1/17 (6)	*	0/12 (0)	⊹	102/304 (34)	2/14 (14)		0/4 (0)	
Hepatitis C		15/116 (13)	0/15 (0)		0/12 (0)		47/304 (15)	1/14 (7)		0/4 (0)	
Without etiology		14/118 (12)	8/16 (50)	***##	12/12 (100)	⊹⊹⊹	67/300 (22)	7/13 (54)	*	3/4 (75)	⊹
non tumor liver Histology	F0-F1	52/118 (44)	16/17 (94)		15/15 (100)		92/192 (48)	9/12 (75)		5/5 (100)	
	F2-F3	36/118 (31)	1/17 (6)	***	0/15 (0)	⊹⊹⊹	29/192 (15)	2/12 (17)	*	0/5 (0)	⊹
	F4	30/118 (25)	0/17 (0)		0/15 (0)		71/192 (37)	1/12 (8)		0/5 (0)	
Abundant fibrous stroma		32/115 (28)	13/18 (72)	*** #	15/15 (100)	⊹⊹⊹	36/323 (11)	6/16 (38)	**	4/6 (67)	⊹⊹
Tumor steatosis		19/100 (19)	10/15 (67)	*** ##	2/13 (15)		105/323 (33)	12/16 (75)	***#	1/6 (17)	
Biliary Tract Invasion		2/104 (2)	5/16 (31)	***	1/13 (8)		7/323 (2)	2/16 (13)		0/6 (0)	
Perineural invasion		0/104 (0)	2/15 (13)	*	2/13 (15)	⊹	0/323 (0)	1/16 (6)	*	1/6 (17)	⊹
Macrotrabecular massive		13/114 (11)	0/13 (0)		0/15 (0)		62/323 (19)	1/16 (6)		0/6 (0)	
Scirrhous pattern		9/117 (8)	3/18 (17)		0/13 (0)		5/319 (2)	0/16 (0)		0/6 (0)	
Lymphocytic inflammation		23/110 (21)	11/15 (73)	*** ##	1/12 (8)		70/323 (22)	8/16 (50)	*	2/6 (33)	
G1G6	G1	13/118 (11)	14/18 (78)		3/15 (20)		41/292 (14)	10/16 (63)		1/6 (17)	
	G2	17/118 (14)	1/18 (6)		0/15 (0)		46/292 (16)	1/16 (6)		0/6 (0)	
	G3	28/118 (24)	1/18 (6)		3/15 (20)		29/292 (10)	0/16 (0)		1/6 (17)	
	G4	22/118 (19)	2/18 (11)	***##	9/15 (60)	⊹⊹	83/292 (28)	3/16 (19)	***	3/6 (50)	
	G5	21/118 (18)	0/18 (0)		0/15 (0)		17/292 (6)	0/16 (0)		0/6 (0)	
	G6	17/118 (14)	0/18 (0)		0/15 (0)		76/292 (26)	2/16 (13)		1/6 (17)	
BAP1 altered		0/118 (0)	18/18 (100)	*** ###	0/15 (0)		0/323 (0)	16/16 (100)	*** ###	0/6 (0)	
CTNNB1 mutated		41/118 (35)	1/18 (6)	*	1/15 (7)	⊹	92/323 (28)	1/16 (6)		0/6 (0)	
TP53 mutated		47/118 (40)	2/18 (11)	*	0/15 (0)	⊹⊹	107/323 (33)	3/16 (19)		0/6 (0)	
TERT altered		63/116 (54)	0/17 (0)	***	2/14 (14)	⊹⊹	89/169 (53)	0/8 (0)	**	2/4 (50)	
DNAJB1-PRKACA fusion		0/118 (0)	0/18 (0)	###	15/15 (100)	⊹⊹⊹	0/323 (0)	0/16 (0)	###	6/6 (100)	⊹⊹⊹

[a] For the TCGA series, only one or two slides were available for histological reviewing

[b] some patients had other etiologies such as hemochromatosis (9 patients with non-BAP1/fusPRKACA tumors and 1 patient with BAP1 tumor) or metabolic syndrome (7 patients with non-BAP1/fusPRKACA tumors and 1 patient with BAP1 tumor)

* BAP1 vs non-BAP1/fusPRKACA (LICA-FR or TCGA cohorts)

BAP1 vs fusPRKACA (LICA-FR)

⊹ fusPRKACA vs non-BAP1/fusPRKACA (LICA-FR)

###, ***, ⊹⊹⊹ p-val < 0.001;   ##, **, ⊹⊹ p-val < 0. 01;   #, *, ⊹ p-val < 0.05

Table 2: Detailed *BAP1* alterations in the 18 patients from the LICA-FR series

Case #	Gender	Age	Histological Diagnosis	Etiology / background	Non tumor liver	*BAP1* genomic alteration (GRCh37, chr3)	BAP1 protein change	*BAP1* copy number variation
#794T[a]	M	73	HCC	Hemochromatosis	F0-F1	52443600del	E31fs	focal del
#1010T	F	53	HCC	Alcohol	F0-F1	52436869_52436870delinsAA	K637*	focal del
#3894T	M	56	HCC	Alcohol	F0-F1	52443876C>A	E7*	focal del
#3907T	M	39	HCC	Alcohol	F0-F1	52441270del	A167fs	focal del
#2135T	F	57	HCC	Alcohol / HBV / NASH	F0-F1	52441301del + 52436304T>G	N157fs + *730C	
#2211T	F	37	HCC	Chronical intrahepatic obstructive cholestasis	F0-F1	52439814_52439830del	VLEANR295fs[b]	focal del
#228T	M	48	HCC	Without etiology	F0-F1	52440294_52440295insTT	Q253fs	focal del
#1182T	F	51	HCC	Without etiology	F0-F1	52442618_52442627del	PA42fs (splice)	large del
#800T	M	73	HCC	Without etiology	F2-F3	52441229del	F181fs	chr3p del
#141T	F	67	HCC	Without etiology	F0-F1	52441252T>C	Y173C	focal del
#412T	F	51	FLC	NA				homozygous del
#411T	F	65	FLC	Alcohol	F0-F1			homozygous del
#3919T	F	54	mixed-FLC/HCC	NA	F0-F1	Inversion (3;3)	Frame-shift fusion	focal del
#4211T	F	40	mixed-FLC/HCC	Without etiology	F0-F1	Translocation t(2;3)	Frame-shift fusion	chr3p del
#026T	F	38	mixed-FLC/HCC	Without etiology	F0-F1	52439136del	P370fs[b]	focal del
#255T	F	39	mixed-FLC/HCC	Without etiology	F0-F1	52441473T>C + 52443758G>A	K127E + G13G (splice)	focal del
#187T	M	27	mixed-FLC/HCC	Without etiology	F0-F1	52441991_52441992del	K120fs[b]	focal del
#906T	F	50	mixed-FLC/HCC	NASH	F0-F1	52443580del	K38fs	focal del

[a] Of note, patient #794T was found outside the cluster of 17 *BAP1* altered tumors (Figure 1) but was later included in the group of BAP1 tumors for further analysis.

[b] 3 mutations were not detected in the first analysis of whole exome sequencing data but were later identified in target sequencing of *BAP1* with a higher depth.

NASH: non alcoholic steatotic hepatitis; HBV: hepatitis B virus; NA: not available

F0-F1: no fibrosis; F2-F3: mild fibrosis; F4: cirrhosis
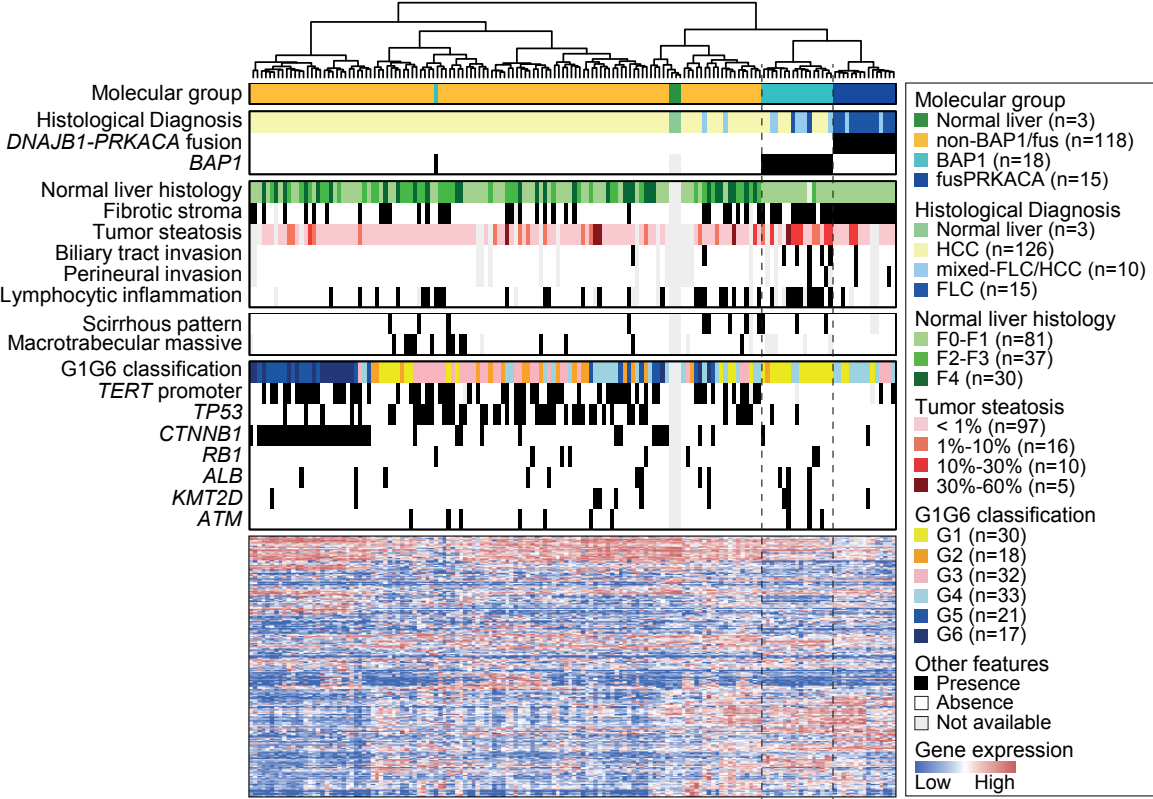
Figure with legends

Figure 1: FLC cluster together and are divided between *BAP1*-driven and *DNAJB1-PRKACA*-driven tumors

Hierarchical clustering based on the expression of the 5000 genes with the higher variability in RNAseq analysis of 151 liver tumors and 3 non-tumor-liver samples. The top heatmaps show clinical, histological and molecular annotation of the samples, while the lower heatmap shows the expression pattern of the 5000 genes.
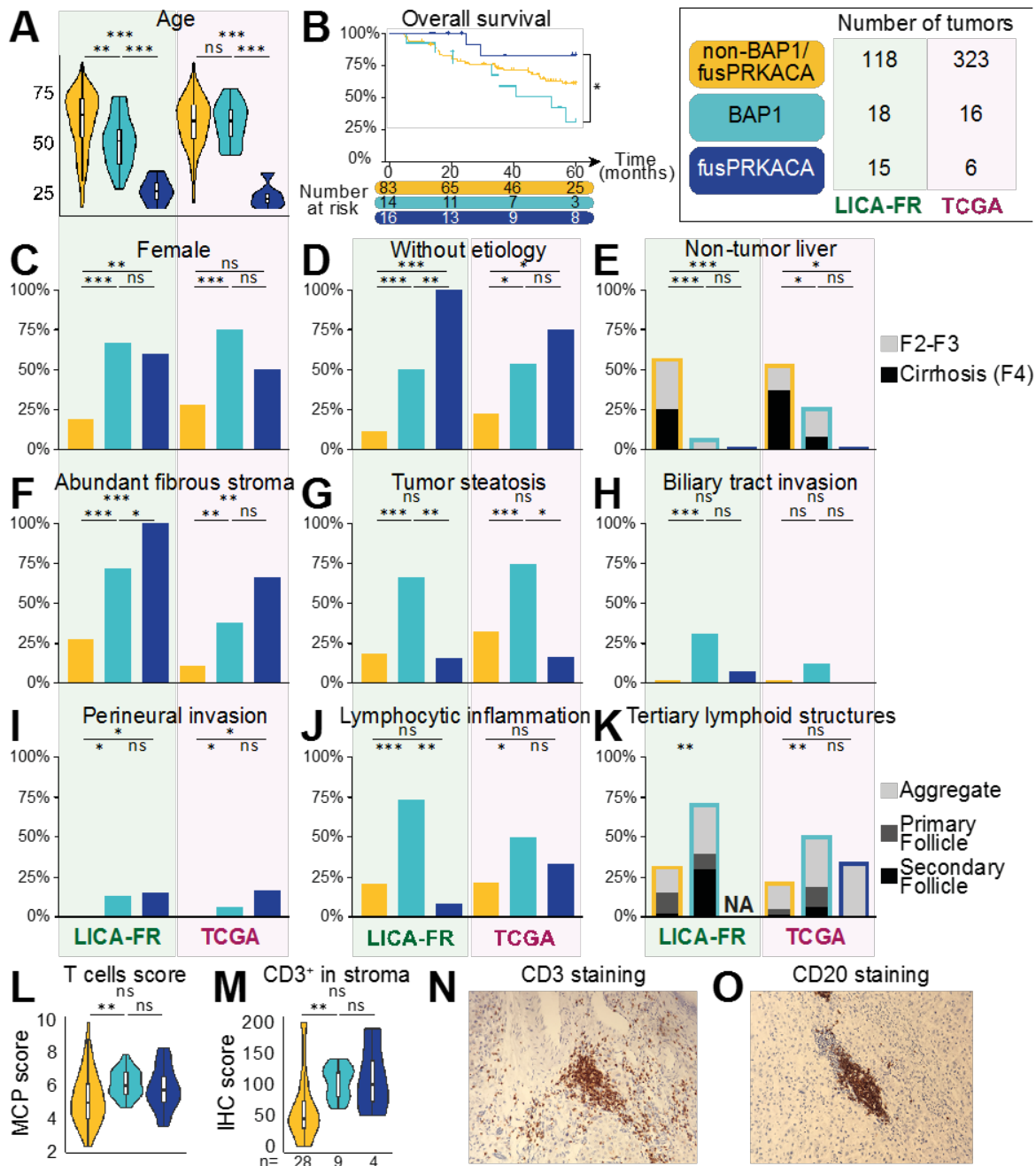
Figure 2: Clinical and histological features of BAP1, fusPRKACA and non-BAP1/fusPRKACA tumors

(A) Distribution of age at surgery. (B) Kaplan-Meier plot showing the overall survival of liver tumors stratified by BAP1 and DNAJB1-PRKACA alterations in the LICA-FR series. (C-E) Repartition of female gender (C), absence of liver disease etiology (D) and non-tumor liver histology (F2-F3: mild fibrosis; F4: cirrhosis) (E). (F-K) Histological reviewing of abundant fibrous stroma (F), tumor steatosis (G), biliary tract invasion (H), perineural invasion (I), lymphocytic inflammation (J) and tertiary lymphoid structures (K). (L) T cell score calculated with the Microenvironment Cell Populations (MCP) counter method applied to RNAseq data of the LICA-FR series. (M) Quantification of T cells abundance in tumor stroma with immunohistochemistry in a subset of tumors from the LICA-FR series. (N, O) Representative images of CD3 (N) and CD20 (O) staining in BAP1 tumors (#411T and #412T respectively), showing the aggregation of T and B cells within aggregate type tertiary lymphoid structures. Wilcoxon test, trend χ² test, Fisher exact test and Log-rank

22

test were used respectively for continuous (A, L), ordinal (C, K), binary (B, D, F-J) and survival data (E): ***p-val < 0.001, **p-val < 0. 01, *p-val < 0.05.
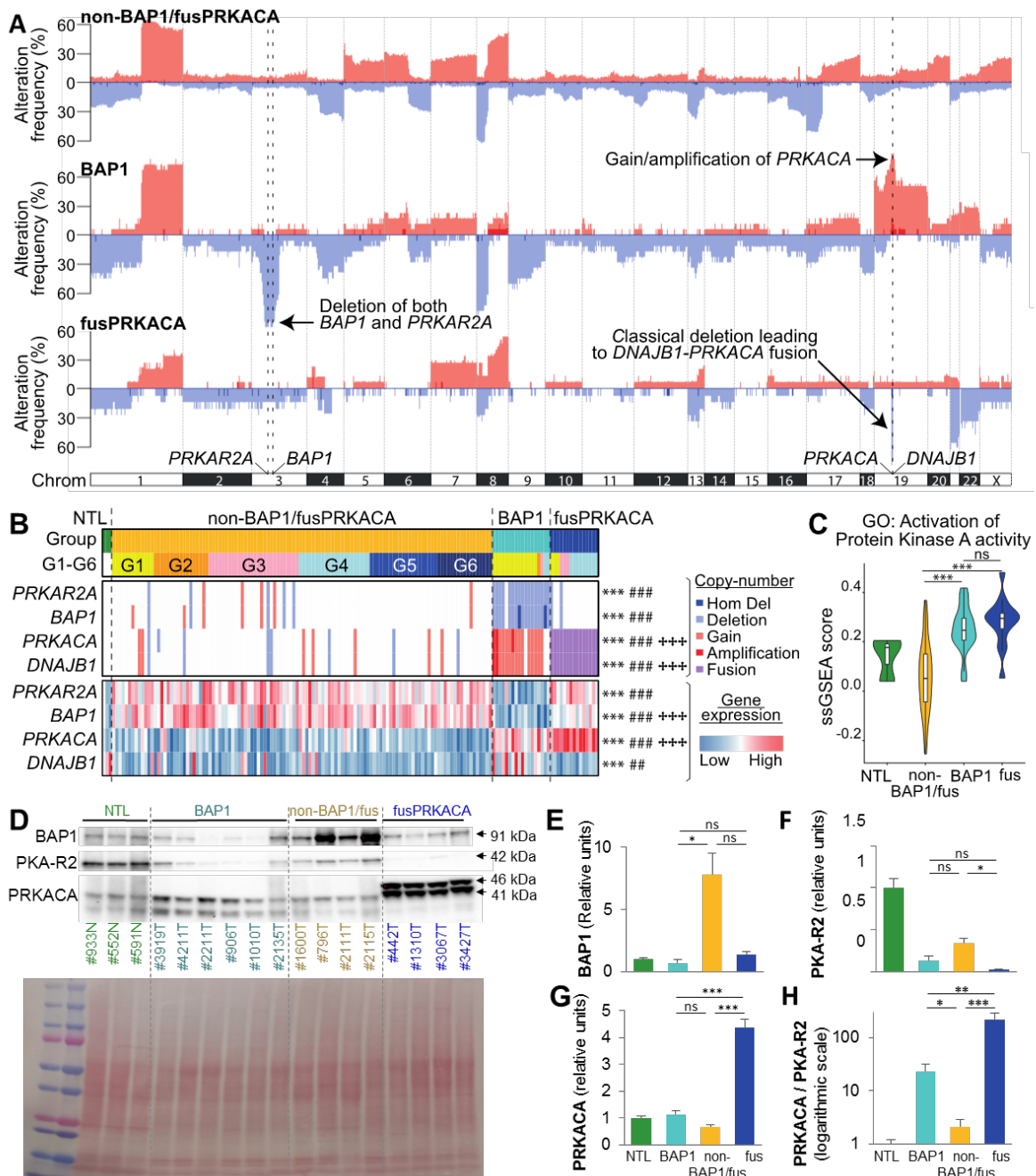

Figure 3: Alternative copy-number alterations activates the PKA pathway in BAP1 tumors

(A) Copy number alterations frequency in the 3 molecular groups of HCC. (B) Heatmap representation of copy-number alterations and relative gene expression for *PRKAR2A*, *BAP1*, *PRKACA* and *DNAJB1* assessed by RNAseq. Statistical comparisons with exact Fisher test (copy number alterations) and Wilcoxon test (gene expression): * BAP1 vs non-BAP1/fusPRKACA, # BAP1 vs fusPRKACA, ╬ fusPRKACA vs non-BAP1/fusPRKACA. (C) Comparison of single sample GSEA scores for the gene set Gene Ontology (GO): Activation of Protein Kinase A activity between the 3 molecular groups of tumors. (D) Western-blot of BAP1, PKA-R2 and PRKACA in normal liver samples (NTL, n=3) and in different liver tumors: BAP1 (n=6), non-BAP1/fusPRKACA (n=4), fusPRKACA (n=4). In fusPRKACA

tumors, the higher mass of the bands stained by the PRKACA antibody corresponds to the already described DNAJB1-PRKACA chimeric protein. Bottom image represents Ponceau coloration. (E-H) Quantification of protein expression of BAP1 (E), PKA-R2 (F), PRKACA (G) and of relative PKA activation measured by the ratio between PRKACA and PKA-R2 (H), compared with Wilcoxon test. *** p-val < 0.001; ** p-val < 0. 01; * p-val < 0.05.
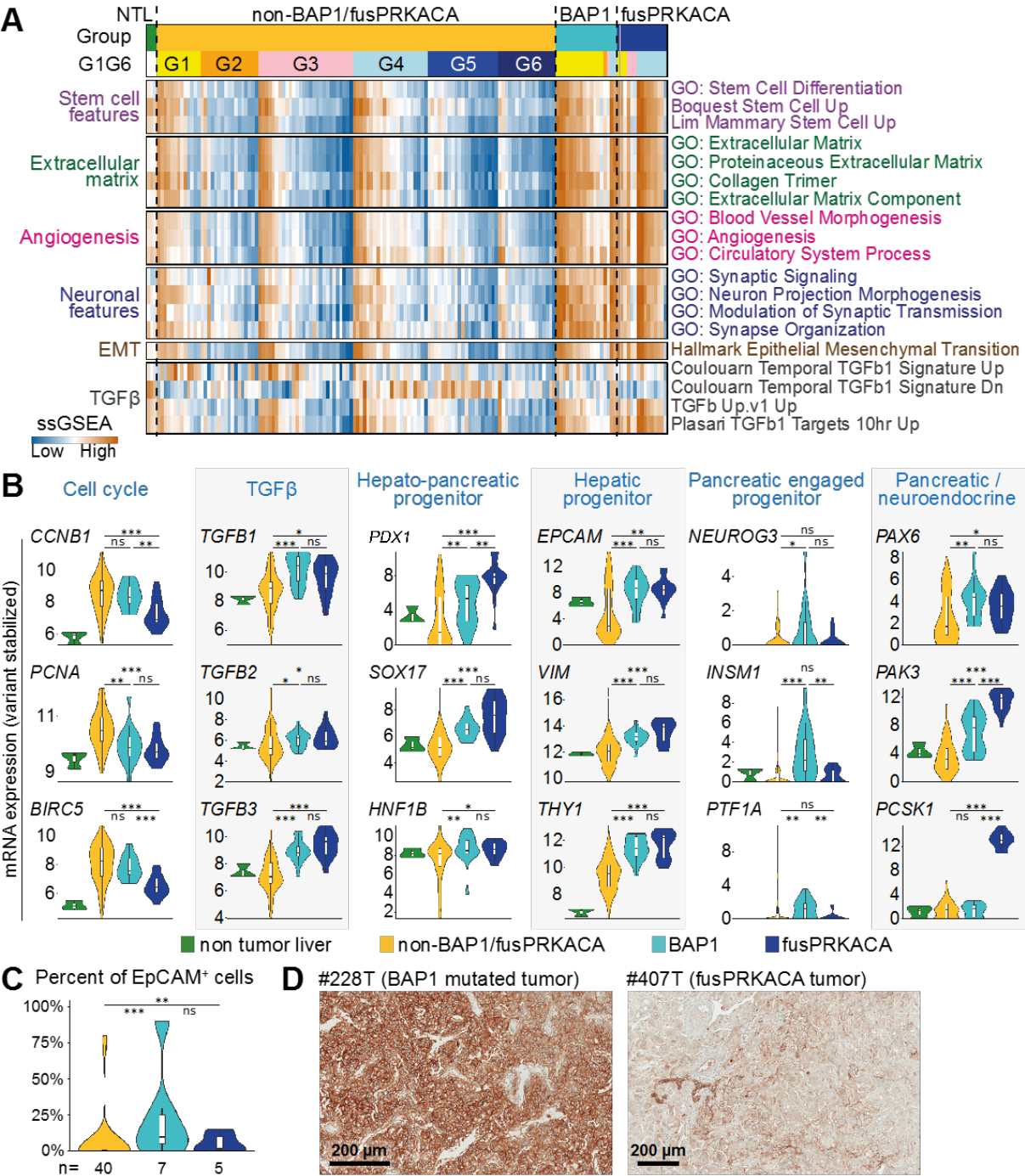

Figure 4: Transcriptomic characterization of BAP1 and fusPRKACA tumors

(A) Heatmap of single sample GSEA for 3 normal liver samples and the different molecular groups of liver tumors ordered by G1-G6 classes. (B) RNAseq expression of representative

24

cell cycle genes, TGFβ ligands as well as representative markers of the different progenitors found in the hepato-pancreatic lineage and of pancreatic / neuroendocrine markers. (C) Immunohistochemistry reveals a higher percentage of EpCAM positive tumor cells in both BAP1 and fusPRKACA tumors. (D) Representative images of EpCAM staining show the lighter staining in fusPRKACA tumors compared to BAP1 tumors. Wilcoxon test: ***p-val < 0.001, **p-val < 0. 01, *p-val < 0.05.
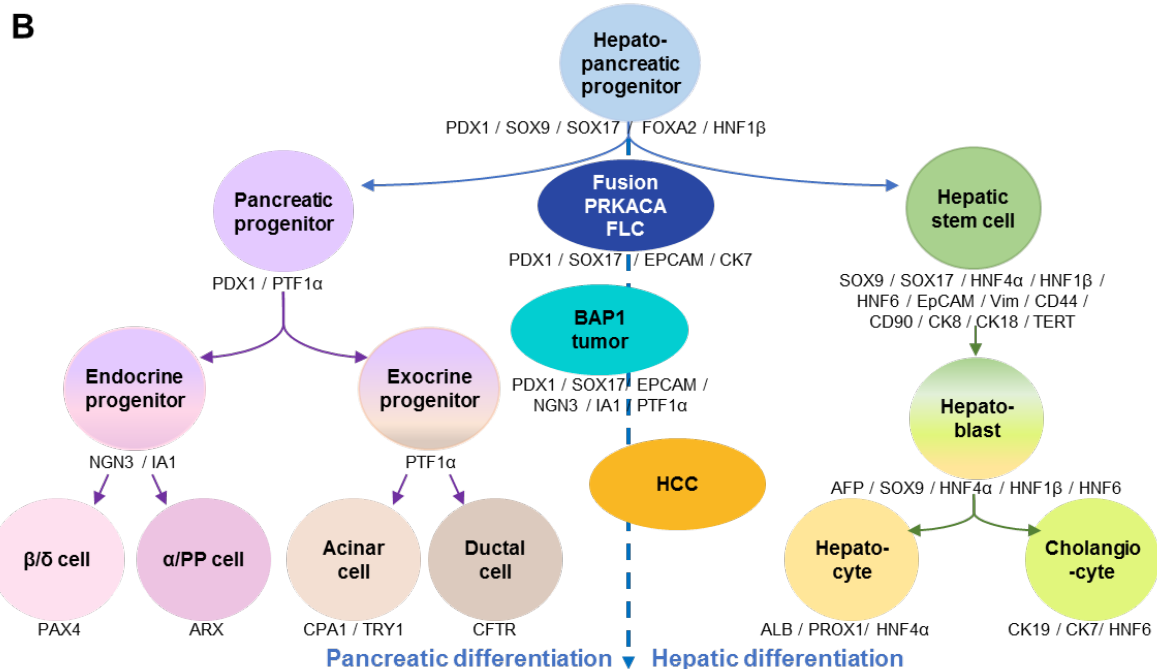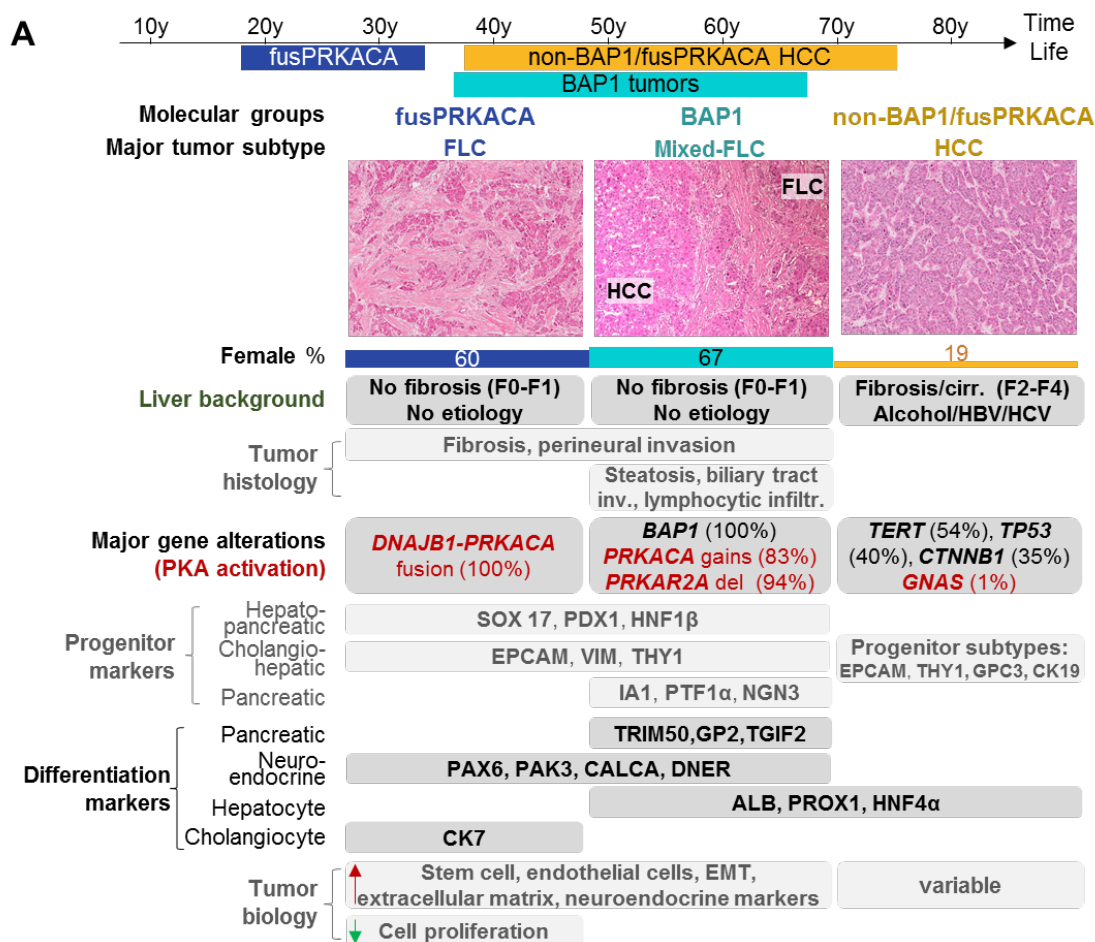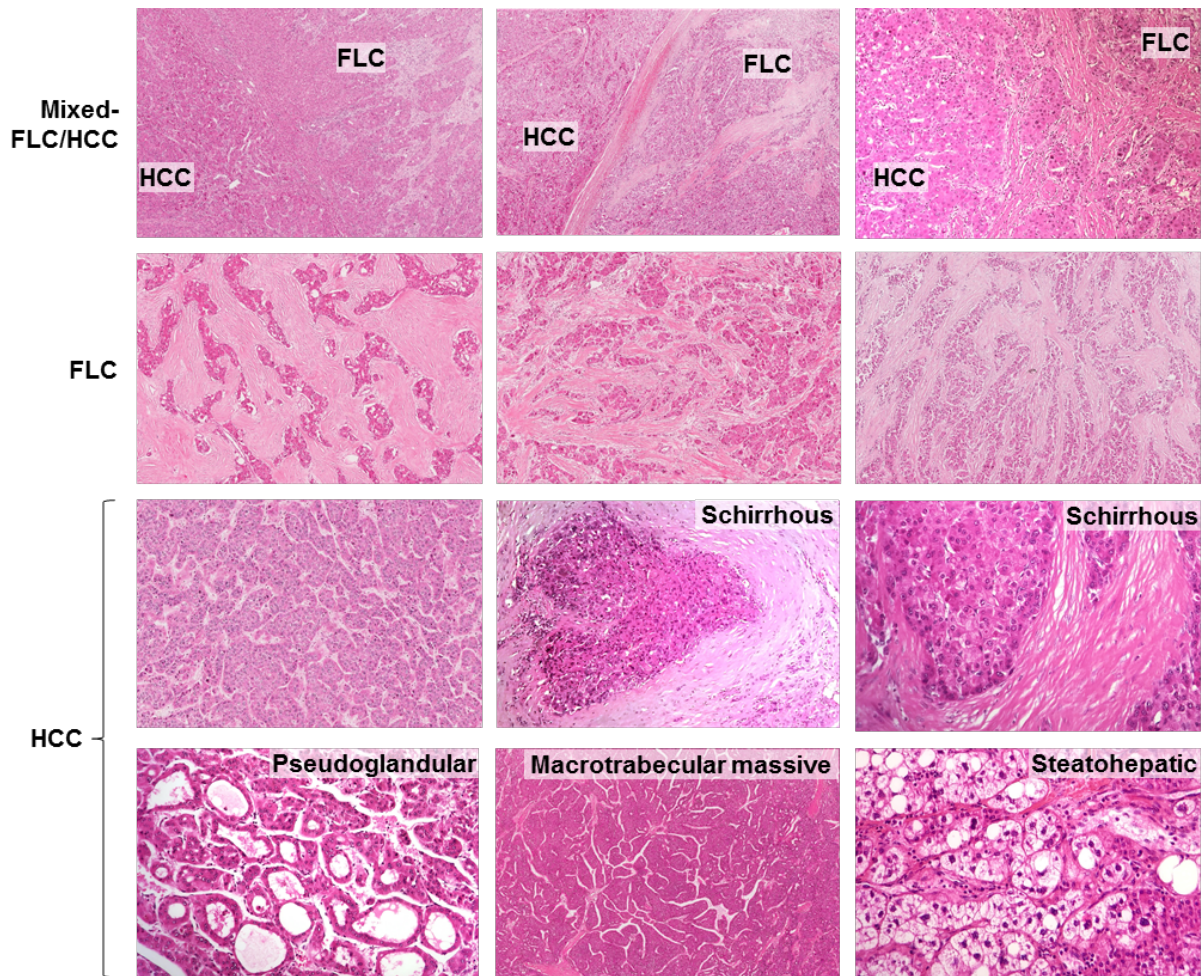
Figure 5: Summarized characteristics of fusPRKACA and BAP1 tumors compared to non-BAP1/fusPRKACA HCC and relation to the common hepato-pancreatic lineage

(A) A recap of the most significant results in terms of histological, clinical and molecular features was represented. Age was represented from the 1st to 9th deciles. (B) Schematic
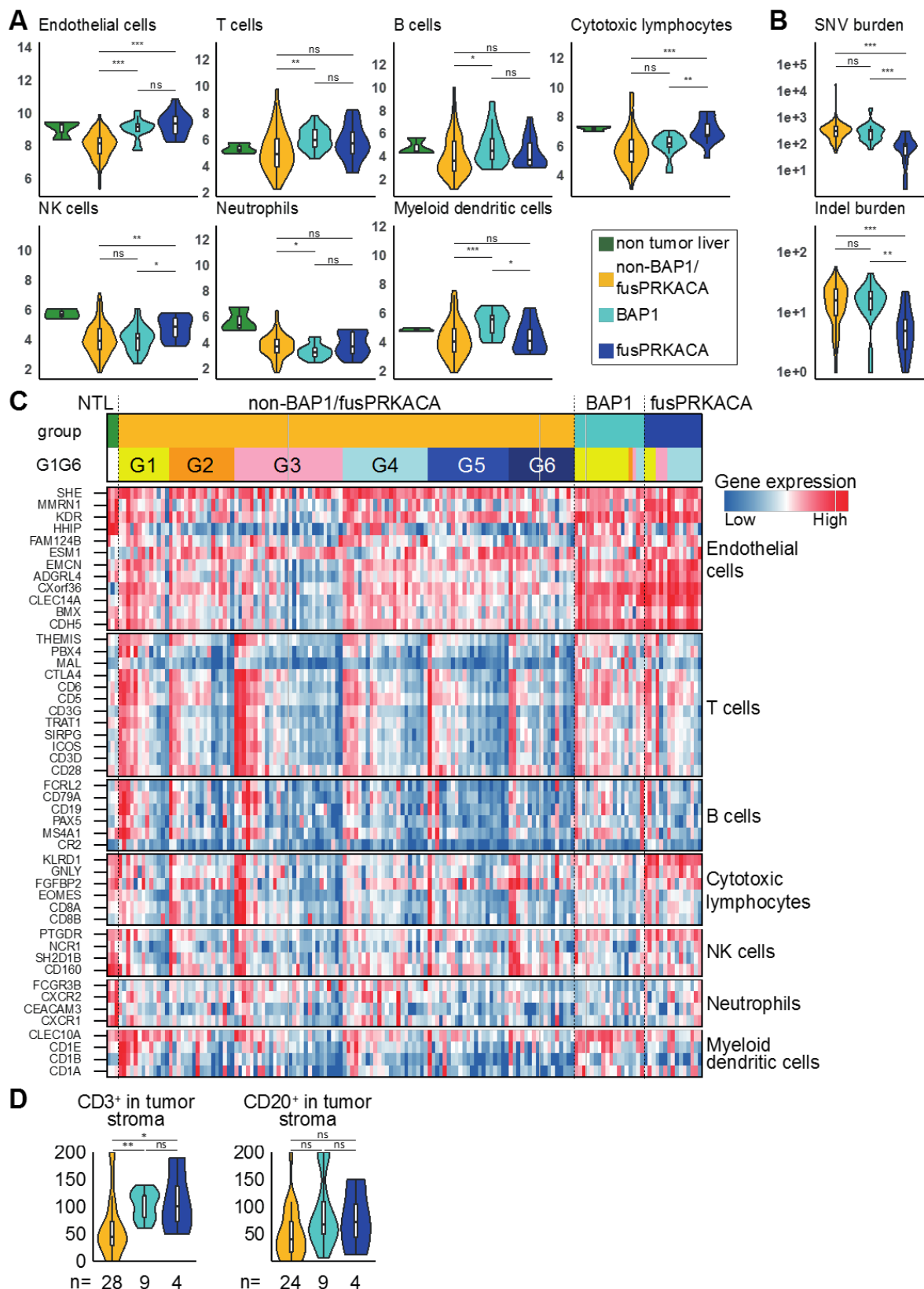
differentiation program from the common hepato-pancreatic progenitor, adapted from Lanzoni et al[40]. FusPRKACA FLC are thought to be directly derived from hepato-pancreatic progenitors found in the young liver while BAP1 tumors have a more pancreatic engaged program.

Supplementary figure legends

Supp Figure 1: Representative hematein-eosin-safran staining of different HCC subtypes
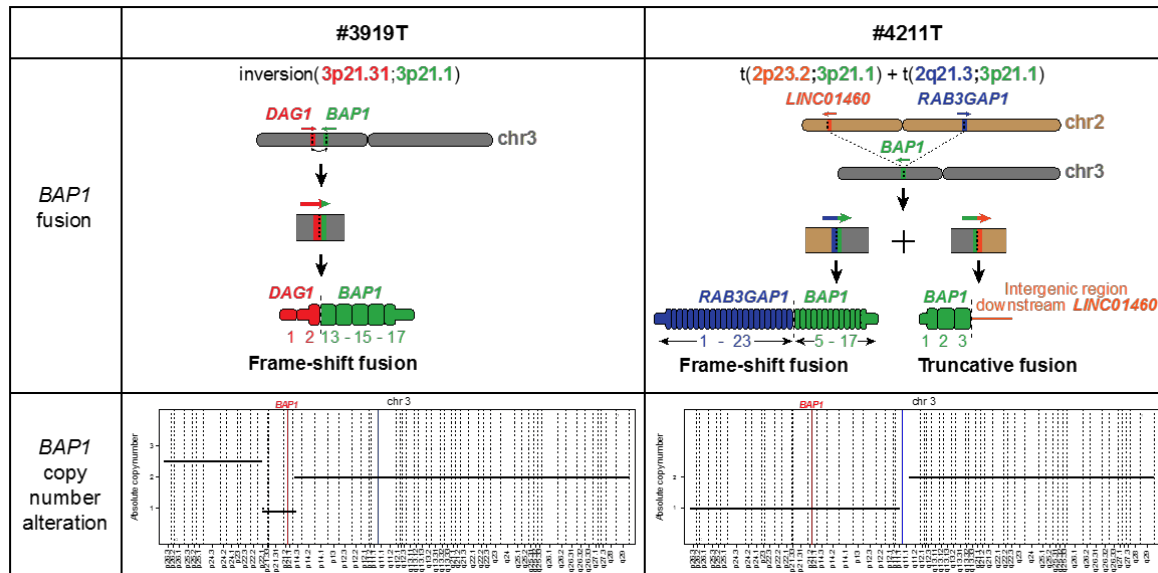
Mixed-FLC/HCC are defined as HCC containing at least one area with FLC features. Examples of distinct histological HCC subtypes (scirrhous, macrotrabecular massive, steatohepatic) as well as pseudoglandular pattern are shown.
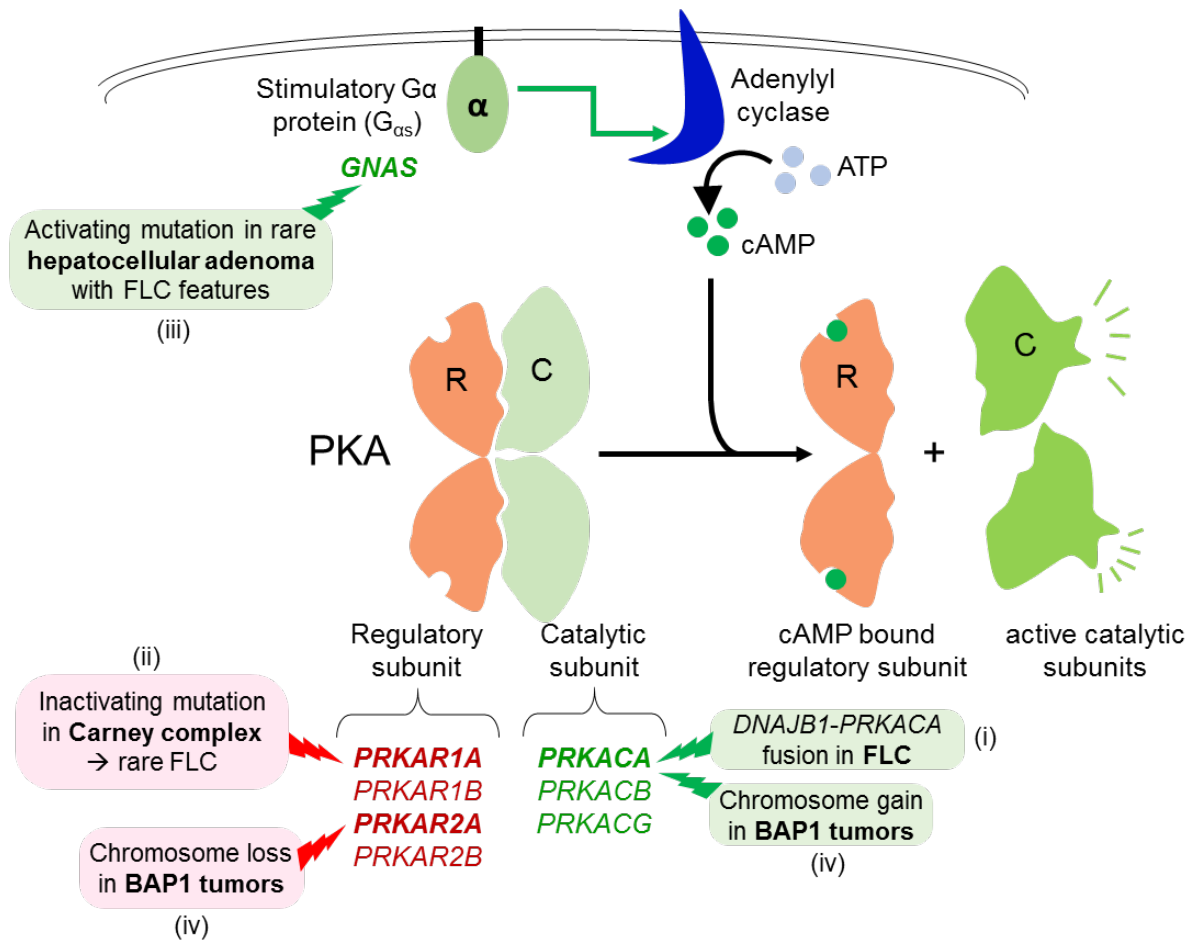
Supp Figure 2: RNAseq analysis of immune infiltrate

(A) Different immune scores calculated with the Microenvironment Cell Populations-counter method applied to RNAseq data. (B) Comparison of the tumor mutational burden (based on the number of mutations in whole-exome-sequencing with a variant allele frequency above 10%) split between single nucleotide variants (SNV, top) and small

insertions and deletions (indel, bottom). (C) Detailed expression of immune related genes used for determining Microenvironment Cell Populations scores in all samples of the LICA-FR cohort, ordered by molecular group, G1-G6 and *CD45* expression. (D) Quantification of CD3+ T cells and CD20+ B cells abundance in tumor stroma. Wilcoxon test: ***p-val < 0.001, **p-val < 0. 01, *p-val < 0.05.
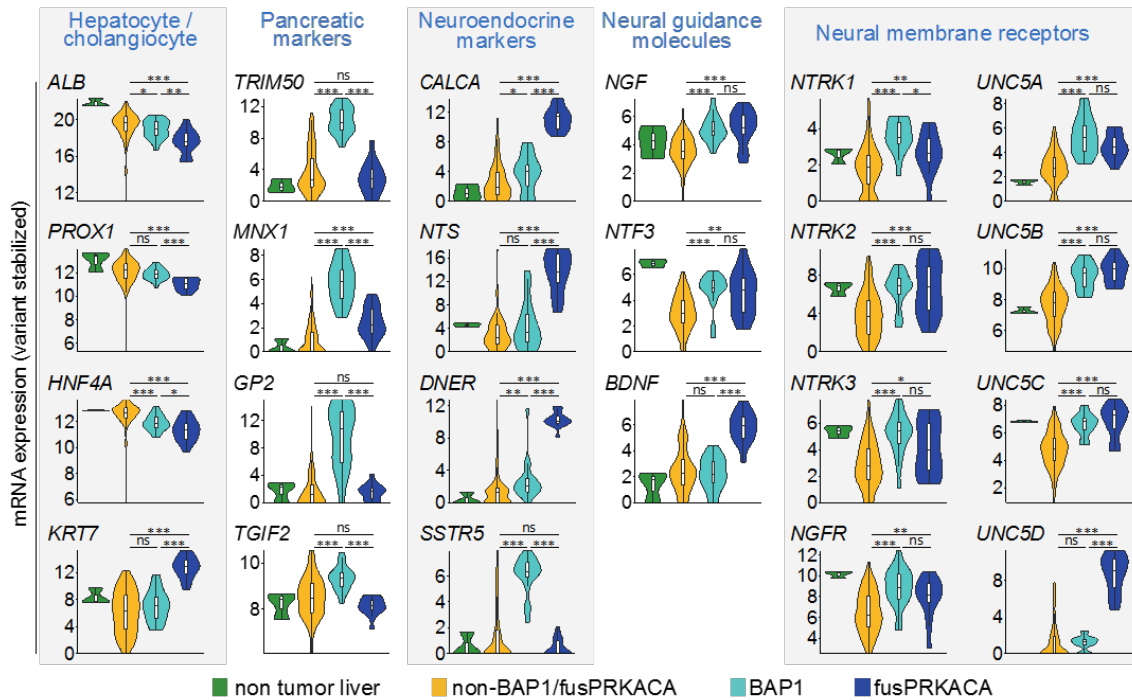

Supp Figure 3: Biallelic inactivation of *BAP1* through gene fusion and copy number alteration in 2 patients

In tumor #3919T, an unbalanced inversion between locus 3p21.31 and 3p21.1 gave rise to a frameshift fusion between *DAG1* and *BAP1* (top panel), while the second *BAP1* allele was lost in a focal deletion (lower panel). In tumor #4211T, a complex event implicating chromosome 2 and 3 led to two translocations, t(2p23.2;3p21.1) and t(2q21.3;3p21.1), with two subsequent gene fusions: a truncative fusion between *BAP1* and the intergenic region downstream to *LINC01460* and a frameshift fusion between *RBA3GAP1* and *BAP1*. The other *BAP1* allele was lost together with the whole 3p arm (lower panel).

Supp Figure 4: Different mechanism of PKA activation in hepatocellular tumors
PKA (cAMP-dependent protein kinase) is composed of regulatory subunits (encoded by genes *PRKAR1A/B* and *PRKAR2A/B*) which normally repress the catalytic subunits (encoded by *PRKACA/B/C*). When cAMP bounds to the regulatory subunits, the catalytic subunits become active. Alpha subunits of stimulatory G-protein ($G_{\alpha s}$, encoded by *GNAS*) activates the adenylyl cyclase, leading to production of cAMP and subsequent activation of PKA. Over-activation of PKA in liver tumors is associated with fibrolamellar features in 4 settings: (i) the *DNAJB1-PRKACA* fusion in FLC, (ii) inactivating mutations in *PRKAR1A* in rare FLC developed in Carney complex patients, (iii) activating mutations in *GNAS* in rare hepatocellular adenomas characterized by fibrolamellar-like patterns and (iv) recurrent gains of *PRKACA* and deletions of *PRKAR2A* in BAP1 tumors.

Supp Figure 5: mRNA expression of lineage and differentiation markers

mRNA expression of markers of hepatocytes, cholangiocytes (*KRT7*), pancreas, neuroendocrine markers, neural guidance molecules and receptors located on the membrane of the neurons assessed by RNAseq in normal liver (n=3), non-BAP1/fusPRKACA (n=118), BAP1 (n=18) and fusPRKACA (n=15) tumors. Wilcoxon test: ***p-val < 0.001, **p-val < 0.01, *p-val < 0.05.